PHYSICAL REVIEW MATERIALS **1**, 061002(R) (2017)

One-dimensional phosphorus chain and two-dimensional blue phosphorene grown on Au(111) by molecular-beam epitaxy

Jin-Peng Xu,[1] Jun-Qiu Zhang,[1] Hao Tian,[1,2] Hu Xu,[2] Wingkin Ho,[1] and Maohai Xie[1,*]

[1]*Department of Physics, Hong Kong University, Hong Kong, China*

[2]*Department of Physics, Southern University of Science and Technology, Shenzhen 518055, China*

(Received 22 May 2017; revised manuscript received 18 August 2017; published 14 November 2017)

Single-layer (SL) phosphorus (phosphorene) has drawn considerable research attention recently as a new two-dimensional (2D) material with great application promises. Blue phosphorus (blueP), an allotrope of black phosphorus, has been suggested to exist in the SL form on some substrates. Here, we report the growth of blueP by molecular-beam epitaxy and reveal an explicit sequential growth behavior that involves a dewetting process of the first adsorbed P atoms in the $(\sqrt{3}\times\sqrt{3})R30^\circ$ patches for the nucleation and growth of SL blueP-like islands. We also reveal a one-dimensional (1D) chain structure at low coverage. Interestingly, over a large coverage range, a composite surface containing locally high-P coverage blueP islands surrounded by locally low-coverage 1D chains prevails over the homogeneous $(\sqrt{3}\times\sqrt{3})R30^\circ$ or P-trimer covered surfaces. Such a phase-separated composite surface is found to be favorable from an energy-minimization point of view and can be general for the growth of other systems.

DOI: 10.1103/PhysRevMaterials.1.061002

After the success of graphene, extensive research effort has been devoted to other two-dimensional (2D) systems. Examples include silicene [1,2], stanene [3,4], borophene [5,6], and group-III and transition-metal dichalcogenides [7–12]. Owing to the superior transport and optical properties, few-layer and single-layer (SL) black phosphorus (BP) has come under the spotlight lately [13–16]. It represents one of the latest members in the expanding 2D family. Blue phosphorus (blueP), an allotrope of BP but arranged in a more flat atomic configuration and having similar appealing properties, has been recently suggested to exist in the SL form on some substrates [17–20]. Blue phosphorene, as it is called, is a semiconductor with a fundamental gap near 2 eV [17]. While BP has been experimentally investigated for exfoliated samples, studies of epitaxial black and blue phosphorene remain scarce.

The typical methods of obtaining few-layer or SL materials include exfoliation, chemical vapor deposition, and molecular-beam epitaxy (MBE). The latter has been shown to be advantageous in producing many designer 2D materials such as silicene [2], stanene [4], and, lately, tellurene [21,22]. It, however, remains challenging to use MBE to grow phosphorene. A recent theoretical study suggested that SL blueP could be stabilized on GaN(0001) via the unusual half-layer by half-layer growth mechanism [19]. There is thus a hope that epitaxial phosphorene can be obtained by MBE, and if so, it would accelerate both the fundamental and practical research of phosphorene films.

In this Rapid Communication, we report the growth of phosphorus by MBE. By using scanning tunneling microscopy (STM), we uncover a one-dimensional (1D) chain structure of P on Au(111). We also observe an explicit sequential growth behavior where the 1D chain develops into $(\sqrt{3}\times\sqrt{3})R30^\circ$ patches before blueP islands nucleate and grow, and the latter invokes a dewetting process of the already adsorbed P atoms in the $(\sqrt{3}\times\sqrt{3})R30^\circ$ patches on the surface. Over a large coverage range, a composite surface prevails where locally high-P coverage blueP islands and low-coverage 1D chains coexist. Such a "phase-separated" surface is in favor over a homogeneous $(\sqrt{3}\times\sqrt{3})R30^\circ$ or P-trimer covered surface due to energy minimization, which can be general for the growth of other similar systems. This finding thus enriches surface growth physics and also provides hints for the epitaxy of various 2D architectures.

Depositions of P and subsequent STM examinations were carried out in a Unisoku UHV system consisted of a sample preparation chamber and an insert of the STM facility operated at 77 K. The base pressure was 1×10^{-10} Torr. Crystalline Au(111) was cleaned by Ar^+ bombardment (1.0 keV, 5×10^{-6} Torr), followed by annealing at ~600 °C. Phosphorus vapor was generated from thermal decomposition of InP in a standard Knudsen cell operated at ~470 °C. The temperature of the substrate was 210–230 °C. After depositing for a preset period, the sample was immediately transferred to the cooling stage of the STM for surface examinations. Electrochemically etched tungsten tips were used, which were conditioned by heating and/or silver decoration. For all the STM measurements, a constant-current mode was used and the tunneling current was 100 pA.

To aid the experiments, the atom adsorption geometry and energy of P on Au(111) were investigated using density functional theory (DFT) calculations. The electronic exchange correlation was treated using the Perdew-Burke-Ernzerhof (PBE) form [23] of the generalized gradient approximation (GGA). The projected augmented wave method [24,25] was employed as implemented in the Vienna *ab initio* simulation package (VASP) [26]. The atom position was optimized by the conjugate gradient method until the forces on each atom were smaller than 0.02 eV/Å. The cutoff energy was 500 eV and the vacuum region was set at ~12 Å. Gamma-centered samplings with $6\times8\times1$ (for a $4\sqrt{3}\times3\sqrt{3}$ supercell), $10\times10\times1$ (for a $3\sqrt{3}\times3\sqrt{3}$ supercell), or $15\times15\times1$ (for a 3×3

*Author to whom correspondence should be addressed: mhxie@hku.hk

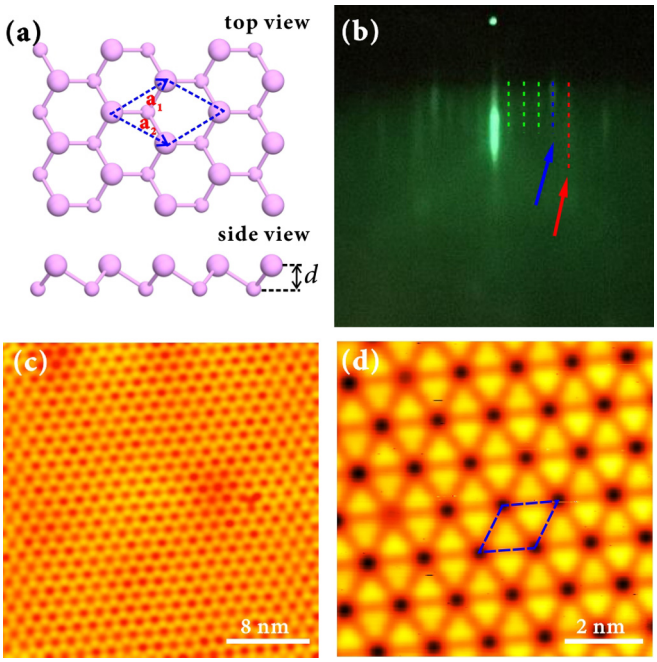

FIG. 1. Blue phosphorene on Au(111). (a) Top view (upper) and side view (lower) of a model of blueP layer. The blue rhombus drawn in the upper panel represents the unit cell. (b) RHEED pattern of epitaxial phosphorene on Au(111). The red and blue arrows point to the 1 × 1 diffraction streaks of the Au substrate and epitaxial P, respectively, and the green dashed lines mark the fraction streaks due to the (5 × 5) reconstruction of the epitaxial P layer. (c) STM topographic image of blueP-like surface (size: 30 × 30 nm^2; sample bias $V_{bias} = 1$ V). (d) A closeup image of the same surface (size: 8 × 8 nm^2; $V_{bias} = 0.1$ V).

supercell) k meshes were used. We employed the DFT-D3 [27] method of Grimme to evaluate the van der Waals (vdW) effect in all calculations. An Au (111) slab with five atomic layers was adopted as the substrate where the bottom layer was fixed to simulate the bulk.

SL blueP has a graphenelike structure but is composed of two atomic layers of P atoms arranged in a buckled honeycomb lattice structure, as illustrated in Fig. 1(a). The unit cell is highlighted by the dashed blue rhombus and the basis vectors $\vec{\mathbf{a}}_1$ and $\vec{\mathbf{a}}_2$ are along the zigzag edges with a lattice constant $a_1 = a_2 = 0.328$ nm [17]. The buckling of blueP defined as the distance between the two P atomic layers is $d \sim 0.13$ nm [28,29]. Figure 1(b) shows a typical reflected high-energy electron diffraction (RHEED) pattern of an epitaxial P layer on Au(111), where the diffraction streaks of Au(111)-1 × 1 and of P are clearly resolved as marked by the red and blue arrows, respectively. Fractional streaks (highlighted by the green dashed lines) are also discernible, suggesting a (4 × 4) superstructure of P that is commensurate with the (5 × 5) supercell of the Au(111) surface. Therefore, the epitaxial P layer has a lattice constant of ∼0.35 nm (i.e., $5a_{Au}/4$, where $a_{Au} \sim 0.288$ nm is the lattice constant of Au). This is considerably larger than the theoretical lattice constant of a free-standing blueP (0.328 nm). So, it would be tensile strained by as much as ∼7% if the epilayer were a blueP SL. Figure 1(c) shows a STM topographic image of the grown P layer, which reveals regularly arranged dark spots in a triangular network. The spatial separation between the neighboring dark spots is exactly five times that of the Au(111) lattice and thus corresponds well with the RHEED observation. Figure 1(d) is a closeup image of the same surface, showing a hexapetalous-flower-like structure where each dark core is surrounded by six triangular bright petals. A similar structure has been reported in Refs. [18,20] and was assigned to be an epitaxial blueP SL. We note that such a reconstructed surface of P on Au is quite stable and persistent. Line profile measurements [see Fig. 2(f) below] indeed suggest it to be a P double layer showing an interlayer distance similar to the buckling height of a blueP SL. Therefore we deduce that the P film is likely a blue phosphorene SL. We, however, would like to remark that the large tensile strain (7%) and the (5 × 5) reconstruction may imply a nonideal blueP, inviting further investigations. On the other hand, the formation of such a blueP-like SL on Au is found to be self-limiting. Prolonged deposition does not lead to thicker films at the conditions used in this experiment.

The main and intriguing finding in this work is the unusual pathway with which the blueP SL is grown. At low coverage, P atoms are seen to aggregate into 1D chains running in three equivalent directions 120° apart, as exemplified in Fig. 2(a). These 1D chains show bright contrasts with an apparent height of 60 pm when measured at a sample bias of 0.1 V. Many chains are seen to branch out or intersect with each other, giving rise to the Y-shaped structure. Mysteriously, star-shaped intersections are rarely found, reflecting some kind of asymmetry or anisotropy in the chain formation kinetics. Such a 1D-chain structure of P on Au(111), as reported here, is similar to a chain structure that was reported for sulfur (S) adsorption on Au(111), where a repulsive pair interaction but an attractive trio interaction of S adatoms was suggested to be responsible for the chain formation [30]. Our own DFT calculations of P adsorbed on Au(111) show a more complicated behavior. At low coverage [$\leqslant 1/9$ monolayers (MLs), where 1 ML is defined as one P adatom per Au(111) surface site], isolated P monomers adsorbed at the fcc sites of Au(111) are more stable than the chemically bonded P trimers. On the other hand, P monomers tend to be closely spaced by occupying the second-nearest-neighbor fcc sites with interatom distances $\sqrt{3}a_{Au}$ apart (refer to the Supplemental Material [31]). Interestingly, at lower coverages ($\leqslant 1/12$ MLs), although the adatom spacing is the same, i.e., $\sqrt{3}a_{Au}$, the chain configuration is found to be more favorable than the close-packed configuration by 18 meV/adatom (see the Supplemental Material [31]), which explains the 1D chains seen for the low-P coverage surfaces, such as those in Fig. 2(a). Figure 2(b) presents a schematic diagram illustrating such a 1D-chain configuration of P on Au(111). A chain-chain separation of $7a_{Au}$ is chosen that corresponds to the average distance of ∼2 nm found from experiment. It translates into a P coverage of $1/(7 \times \sqrt{3}) \approx 1/12$ MLs. The preferred chain configuration of P adatoms at low coverages reflects an effect of P-adatom, chain, and substrate interactions via structural relaxation or a charge transfer effect.

Increasing P dosage causes the surface to become covered by more compactly arranged spots with a hexagonal structure as exemplified in Fig. 2(c). There are, however,

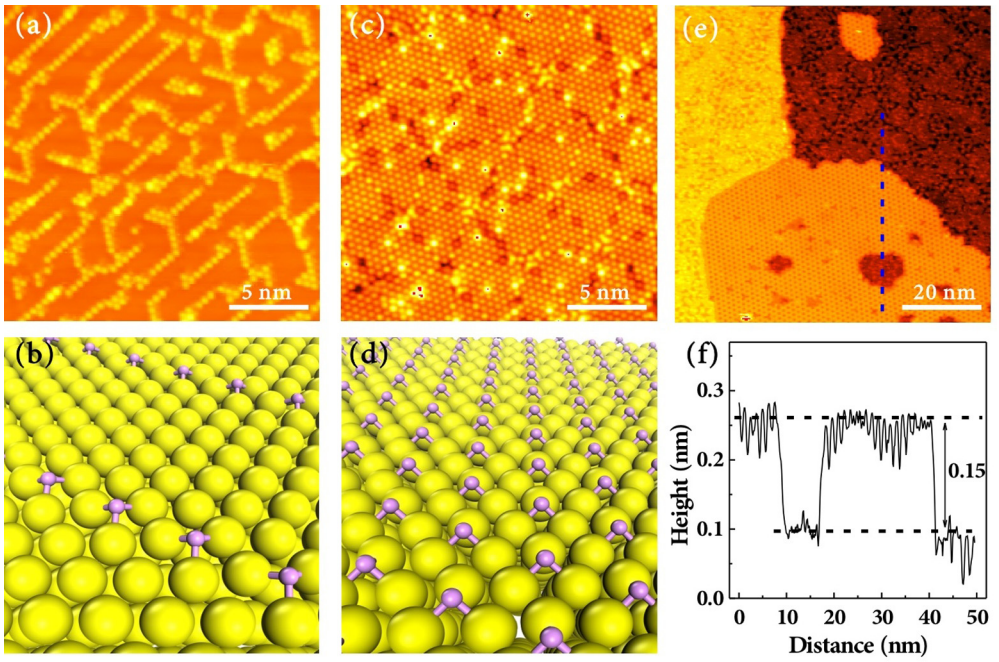

FIG. 2. Growth sequence of epitaxial blueP. (a) STM image (size: $20 \times 20\,\mathrm{nm}^2$; $V_{\mathrm{bias}} = 0.1\,\mathrm{V}$) of a surface after exposing the Au(111) surface to a low dosage of P. (b) Schematic diagram illustrating the 1D-chain configuration of adsorbed P atoms (small pink balls) on Au(111) (yellow balls). Each P atom is anchored on a fcc site and the nearest P atoms are $\sqrt{3}a_{\mathrm{Au}}$ apart. (c) STM image (size: $20 \times 20\,\mathrm{nm}^2$; $V_{\mathrm{bias}} = 0.1\,\mathrm{V}$) of a surface at higher P dosage showing a more closely packed $(\sqrt{3} \times \sqrt{3})R30^\circ$ structure. (d) Schematic diagram illustrating the $(\sqrt{3} \times \sqrt{3})R30^\circ$ reconstructed surface. (e) STM image (size: $80 \times 80\,\mathrm{nm}^2$; $V_{\mathrm{bias}} = 0.1\,\mathrm{V}$) of a surface containing mixed regions of $(\sqrt{3} \times \sqrt{3})R30^\circ$ and blueP. Note also the $(\sqrt{3} \times \sqrt{3})R30^\circ$-structured hole within the blueP terrace. (f) Line profile taken along the vertical blue dashed line in (e), revealing the buckling height of blueP.

apparent domain walls delineating domains of sizes ∼5 nm. The latter indicates the film to be unsteady and perhaps readily transformed into other more thermodynamically stable configurations. Figure 2(d) illustrates schematically such a surface at 1/3 ML coverage showing a hexagonal lattice of P adatoms and a lattice constant of $\sqrt{3}a_{\mathrm{Au}}$. We refer to it as the $(\sqrt{3} \times \sqrt{3})R30^\circ$ reconstructed surface. It is obviously one atomic layer high and evolved from the 1D chain with increasing P coverage. Our DFT calculations indeed reveal that at coverages greater than $\geq 1/9$ MLs, the energy difference between the 1D-chain and close-packed $(\sqrt{3} \times \sqrt{3})R30^\circ$ surfaces becomes minimal. So the chain structure gradually evolves into more compact $(\sqrt{3} \times \sqrt{3})R30^\circ$ patches and finally one of the whole surface being $(\sqrt{3} \times \sqrt{3})R30^\circ$ reconstructed at a coverage of 1/3 MLs.

Increasing P coverage further to above 1/3 MLs, our calculations (refer to Fig. S1 in the Supplemental Material) as well as that of others [19] suggest an evolution of the surface towards a P-trimer covered one, and at coverages >1 ML SL blueP. Experimentally, we, however, have never captured the P-trimer surface. In fact, we even seldom capture surfaces of compact $(\sqrt{3} \times \sqrt{3})R30^\circ$ over large areas. Instead, we often observe blueP islands or patches formed in the background of loose $(\sqrt{3} \times \sqrt{3})R30^\circ$ patches or 1D chains. Figure 2(e) shows a STM image of such a surface, where an isolated blueP island and a blueP patch are seen to coexist with the loose $(\sqrt{3} \times \sqrt{3})R30^\circ$ structure in the background. As described earlier, blueP on Au(111) is characterized by a hexapetalous-flower-like structure and the (5×5) periodicity of the dark cores [18,20]. A line profile measurement across the blueP patch [Fig. 2(f)] reveals a step height of 0.15 nm of blueP above the loose $(\sqrt{3} \times \sqrt{3})R30^\circ$ terrace. This agrees well with the buckling height of a blue phosphorene SL [i.e., 0.13 nm when measured from the top to bottom layer P atoms; refer to Fig. 1(a)]. In Fig. 2(e), one also finds unfilled holes within the blueP patch, and close examinations of such holes reveal the same $(\sqrt{3} \times \sqrt{3})R30^\circ$ structure as well as the step height of ∼0.15 nm. Therefore, it is reasonable to suggest that blueP nucleates by adsorbing the second-layer P atoms on top of the first-layer P atoms characterized by $(\sqrt{3} \times \sqrt{3})R30^\circ$ reconstruction.

There is a discontinuous jump in local P coverage from the $(\sqrt{3} \times \sqrt{3})R30^\circ$ structure (∼1/3 MLs) to blueP (∼2 MLs). By conventional view of surface growth processes and DFT calculations, we expect a gradual evolution of the surface with increasing P coverage, from 1D chains, $(\sqrt{3} \times \sqrt{3})R30^\circ$ patches, P trimers, and finally to blueP. It is thus surprising to note an abrupt change from the $(\sqrt{3} \times \sqrt{3})R30^\circ$ surface directly to blueP. It requires a substantial amount of P atoms to facilitate such a change. These additional P atoms have to come from sources other than just the flux. By examining the $(\sqrt{3} \times \sqrt{3})R30^\circ$ terraces of Figs. 2(c) and 2(e), one notes that the structure is much looser in the latter, which points to the possibility that blueP nucleates by consuming P atoms in the otherwise compact $(\sqrt{3} \times \sqrt{3})R30^\circ$ regions nearby. In fact, we observe many cases where blueP islands

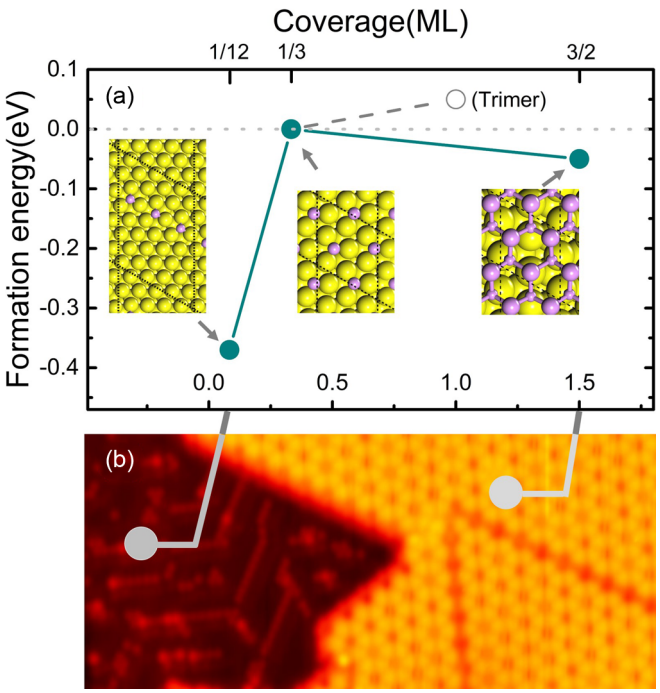

FIG. 3. Phase-separated composite surface. (a) Relative formation energies per P adatom of some stable configurations (insets) of P on Au(111), i.e., 1D chain, compact $(\sqrt{3}\times\sqrt{3})R30^\circ$, P-trimer, and blueP, at different coverages. The formation energy E_f is defined as $E_f = (E_t - E_{\text{sub}})/N$, where N is the number of P adatoms, E_t is the total energy, and E_{sub} is that of the substrate. The E_f of the $(\sqrt{3}\times\sqrt{3})R30^\circ$ structure is set at zero. The yellow and purple balls in the inset represent Au and P atoms, respectively. For P atoms in blueP, the ball size marks the vertical position where the larger balls represent higher positions. (b) STM image (size: $31\times14\,\text{nm}^2$; $V_{\text{bias}} = 0.1\,\text{V}$) showing locally low-coverage 1D chains (left) surrounding the high-coverage blueP island/terrace (right).

or patches are surrounded by 1D chains instead of the loose $(\sqrt{3}\times\sqrt{3})R30^\circ$ patches [refer to Fig. 3(b) below]. This growth behavior resembles a dewetting growth process that has been observed in some other systems where multilayers grow at the expense of the already formed monolayer [32–35]. For P growth on Au(111), the $(\sqrt{3}\times\sqrt{3})R30^\circ$ patch is, however, not completely consumed and the nucleation islands are of blueP SL. The latter does not form until almost the whole surface becomes covered by the $(\sqrt{3}\times\sqrt{3})R30^\circ$ structure at a coverage $\sim 1/3$ MLs.

The finding that a composite surface containing local high-coverage blueP surrounded by local low-coverage loose $(\sqrt{3}\times\sqrt{3})R30^\circ$ patches or 1D chains is in favor of a homogeneous compact $(\sqrt{3}\times\sqrt{3})R30^\circ$ or P-trimer covered surface is intriguing. It may be viewed as a phase separation of the latter into coexisting blueP and loose $(\sqrt{3}\times\sqrt{3})R30^\circ$ regions with the overall P coverage being maintained. This happens by a reduction in system energy. To illustrate this, we plot in Fig. 3(a) the calculated formation energies of 1D-chain, compact $(\sqrt{3}\times\sqrt{3})R30^\circ$, P-trimer, and blueP configurations, which are stable at the respective coverages (refer to the Supplemental Material [31]). As seen, the $(\sqrt{3}\times\sqrt{3})R30^\circ$ and P-trimer surfaces both have higher formation energies than the 1D-chain and blueP structures. Therefore, as P coverage builds up, instead of forming compact $(\sqrt{3}\times\sqrt{3})R30^\circ$ or P-trimer structures over large surface areas, fluctuation may cause blueP to nucleate and grow in certain places, consuming the P adatoms in the already formed $(\sqrt{3}\times\sqrt{3})R30^\circ$ patches and in return converting the latter into the loose $(\sqrt{3}\times\sqrt{3})R30^\circ$ or 1D-chain structure. BlueP surrounded by 1D chains is exemplified in the STM image of Fig. 3(b).

In summary, we demonstrate P growth on Au(111) by MBE and discover a 1D-chain structure of P on Au(111). These 1D chains evolve into $(\sqrt{3}\times\sqrt{3})R30^\circ$ patches before blueP-like islands nucleate. Before a compact $(\sqrt{3}\times\sqrt{3})R30^\circ$ or P-trimer surface is practically realized over large areas, local fluctuations lead to the nucleation of blueP in certain regions by consuming some of the P atoms in the already formed $(\sqrt{3}\times\sqrt{3})R30^\circ$, converting the latter into more dilute P structures such as loose $(\sqrt{3}\times\sqrt{3})R30^\circ$ patches or 1D chains. Thus blueP formation involves a dewetting process of the first deposited submonolayer P. It then leads to a composite surface containing the low-coverage regions surrounding the high-coverage blueP islands. Such a growth characteristic is driven by energy minimization and can be general for the growth of other similar systems.

This work was financially supported by a Collaborative Research Fund (HKU9/CRF/13G) sponsored by the Research Grants Council (RGC), Hong Kong Special Administrative Region.

J.-P.X., J.-Q.Z., and H.T. contributed equally to this work.

[1] P. Vogt, P. De Padova, C. Quaresima, J. Avila, E. Frantzeskakis, M. C. Asensio, A. Resta, B. Ealet, and G. Le Lay, Phys. Rev. Lett. **108**, 155501 (2012).

[2] L. Chen, C. C. Liu, B. J. Feng, X. Y. He, P. Cheng, Z. J. Ding, S. Meng, Y. G. Yao, and K. H. Wu, Phys. Rev. Lett. **109**, 056804 (2012).

[3] Y. Xu, B. Yan, H.-J. Zhang, J. Wang, G. Xu, P. Tang, W. Duan, and S.-C. Zhang, Phys. Rev. Lett. **111**, 136804 (2013).

[4] F. F. Zhu, W. J. Chen, Y. Xu, C. L. Gao, D. D. Guan, C. H. Liu, D. Qian, S. C. Zhang, and J. F. Jia, Nat. Mater. **14**, 1020 (2015).

[5] X.-F. Zhou, X. Dong, A. R. Oganov, Q. Zhu, Y. Tian, and H.-T. Wang, Phys. Rev. Lett. **112**, 085502 (2014).

[6] A. J. Mannix, X. F. Zhou, B. Kiraly, J. D. Wood, D. Alducin, B. D. Myers, X. L. Liu, B. L. Fisher, U. Santiago, J. R. Guest, M. J. Yacaman, A. Ponce, A. R. Oganov, M. C. Hersam, and N. P. Guisinger, Science **350**, 1513 (2015).

[7] P. Hu, Z. Wen, L. Wang, P. Tan, and K. Xiao, ACS Nano **6**, 5988 (2012).

[8] D. A. Bandurin, A. V. Tyurnina, G. L. Yu, A. Mishchenko, V. Zólyomi, S. V. Morozov, R. K. Kumar, R. V. Gorbachev, Z. R. Kudrynskyi, S. Pezzini *et al.*, Nat. Nanotechnol. **12**, 223 (2017).

[9] K. F. Mak, C. Lee, J. Hone, J. Shan, and T. F. Heinz, Phys. Rev. Lett. **105**, 136805 (2010).

[10] Q. H. Wang, K. Kalantar-Zadeh, A. Kis, J. N. Coleman, and M. S. Strano, Nat. Nanotechnol. **7**, 699 (2012).
[11] X. Xu, W. Yao, D. Xiao, and T. F. Heinz, Nat. Phys. **10**, 343 (2014).
[12] H. Liu, L. Jiao, F. Yang, Y. Cai, X. Wu, W. Ho, C. Gao, J. Jia, N. Wang, H. Fan, W. Yao, and M. Xie, Phys. Rev. Lett. **113**, 066105 (2014).
[13] H. Liu, A. T. Neal, Z. Zhu, Z. Luo, X. F. Xu, D. Tomanek, and P. D. Ye, ACS Nano **8**, 4033 (2014).
[14] V. Tran, R. Soklaski, Y. Liang, and L. Yang, Phys. Rev. B **89**, 235319 (2014).
[15] L. Li, Y. Yu, G. J. Ye, Q. Ge, X. Ou, H. Wu, D. Feng, X. H. Chen, and Y. Zhang, Nat. Nanotechnol. **9**, 372 (2014).
[16] F. Xia, H. Wang, and Y. Jia, Nat. Commun. **5**, 4458 (2014).
[17] Z. Zhu and D. Tománek, Phys. Rev. Lett. **112**, 176802 (2014).
[18] J. L. Zhang, S. Zhao, C. Han, Z. Wang, S. Zhong, S. Sun, R. Guo, X. Zhou, C. D. Gu, and K. D. Yuan, Nano Lett. **16**, 4903 (2016).
[19] J. Zeng, P. Cui, and Z. Zhang, Phys. Rev. Lett. **118**, 046101 (2017).
[20] C. Gu, S. Zhao, J. L. Zhang, S. Sun, K. Yuan, Z. Hu, C. Han, Z. Ma, L. Wang, F. Huo *et al.*, ACS Nano **11**, 4943 (2017).
[21] X. Huang, J. Guan, Z. Lin, B. Liu, S. Xing, W. Wang, and J. Guo, Nano Lett. **17**, 4619 (2017).
[22] J. Chen, Y. Dai, Y. Ma, X. Dai, W. Ho, and M. Xie, Nanoscale (2017), doi:10.1039/C7NR04085G.
[23] J. P. Perdew, K. Burke, and M. Ernzerhof, Phys. Rev. Lett. **77**, 3865 (1996).
[24] P. E. Blochl, Phys. Rev. B **50**, 17953 (1994).
[25] G. Kresse and D. Joubert, Phys. Rev. B **59**, 1758 (1999).
[26] G. Kresse and J. Furthmuller, Phys. Rev. B **54**, 11169 (1996).
[27] S. Grimme, J. Antony, S. Ehrlich, and H. Krieg, J. Chem. Phys. **132**, 154104 (2010).
[28] Y. Mogulkoc, M. Modarresi, A. Mogulkoc, and Y. Ciftci, Comput. Mater. Sci. **124**, 23 (2016).
[29] B. Ghosh, S. Nahas, S. Bhowmick, and A. Agarwal, Phys. Rev. B **91**, 115433 (2015).
[30] H. Walen, D.-J. Liu, J. Oh, H. Lim, J. W. Evans, Y. Kim, and P. A. Thiel, J. Chem. Phys. **143**, 014704 (2015).
[31] See Supplemental Material at http://link.aps.org/supplemental/10.1103/PhysRevMaterials.1.061002 for further information on the DFT results of formation energies of various configurations.
[32] S. A. Burke, W. Ji, J. M. Mativetsky, J. M. Topple, S. Fostner, H.-J. Gao, H. Guo, and P. Grütter, Phys. Rev. Lett. **100**, 186104 (2008).
[33] E. Le Moal, M. Müller, O. Bauer, and M. Sokolowski, Phys. Rev. B **82**, 045301 (2010).
[34] J. L. Neff, P. Milde, C. Perez Leon, M. D. Kundrat, L. M. Eng, C. R. Jacob, and R. Hoffmann-Vogel, ACS Nano **8**, 3294 (2014).
[35] Y. R. Niu, K. L. Man, A. Pavlovska, E. Bauer, and M. S. Altman, Phys. Rev. B **95**, 064404 (2017).